THERMAL AND IN-REACTOR DENSIFICATION OF UO^2: MECHANISMS AND EXPERIMENTAL RESULTS

H. ASSMANN, H. STEHLE

Kraftwerk Union AG, Reaktortechnik,
D-8520 Erlangen, Germany

SUMMARY

The modelling of fuel behaviour during irradiation and the tailoring of an irradiation stable fuel require an accurate description of the stress free volume changes due to fuel densification and fuel swelling. The influence of fuel flow due to creep and hot pressing should be considered separately. This paper presents detailed densification models which describe the dependence of densification on time or burnup, temperature, density, pore size distribution, grain size, and fission rate. UO_2 matrix swelling due to fission product accumulation and densification due to pore shrinkage are considered to operate simultaneously and are linearly superposed.

Densification is in principle a two step mechanism: (1) generation of an excess vacancy concentration around the pores, and (2) migration of these vacancies along the concentration gradient from the sources to the sinks, e.g. grain boundaries. Excess vacancy generation is thermally activated as well as fission induced, but at low temperatures the fission induced generation exceeds the thermal generation. The vacancy migration is purely thermally activated except at very low temperatures, where an athermal irradiation component of migration exists.

Based on these processes, four temperature regions can be identified which describe the dependence of irradiation induced fuel densification on temperature. These are:

Region I : Totally athermal densification below $\approx 450°C$.

Region II : Densification depends on temperature in the region $\approx 450°C \leqq T \leqq \approx 750°C$, where thermally activated vacancy migration is rate controlling.

Region III : Densification is independent of temperature in the region $\approx 750°C \leqq T \leqq \approx 1\,300°C$, where athermal excess vacancy generation by fission spike pore overlap mechanisms are rate controlling.

Region IV : Totally thermally activated densification above $\approx 1\,300°C$.

The shrinkage rate of small pores strongly controls the initial densification rate. Coarser intragranular pores act as ineffective vacancy sinks during this initial stage. The pore size distribution will change. Smaller pores will shrink more rapidly than larger pores while medium size pores, which can also act as vacancy sinks, can possibly swell.

Grain size is of minor importance in the high temperature region especially if the pore concentration is low. At low temperatures and high pore concentration the fraction of excess vacancies which read the grain boundaries decreases with increasing grain size. Therefore, in general, large grain size material is more densification resistant.

Experimental verification of the densification models is obtained from numerous constant temperature thermal sinter tests conducted between 1 200°C and 1 900°C (region IV) as well as in isothermal irradiation tests between 1 000°C and 1 200°C (region III) and around 700°C (region II). Nearly all important features of the densification models have been qualitatively confirmed in the comprehensive experimental program sponsored by EEI/EPRI/Nuclear Industry and reported by M. D. Freshley et. al.: *Irradiation-Induced Densification of* UO_2*Pellet Fuel,* J. Nucl. Mat. 62 (1976) 138–166.

Although the kinetics of thermal and in-reactor densification are different, standardized thermal resinter tests can be established and used to predict the in-reactor densification.

1. Introduction

This paper reviews the densification behaviour of sintered UO_2 pellets and could be applied to other fissionable materials as well. Quantitative description of fuel densification and swelling is required for: (1) identification of limiting properties, (2) modeling and prediction of fuel performance under irradiation, and (3) "tailoring" of an optimized fuel microstructure. Both, densification by shrinkage of pores and matrix swelling due to fission products operate simultaneously and are linearly superimposed.

2. Densification Mechanisms and Models

Pure thermally activated densification was first analyzed 1961 by Coble [1], who described the final stage sintering of dense particles (tetradecahedrons) with intergranular pores. A modified model which considers the realistic microstructure of ceramic bodies (extended intragranular porosity) was introduced by Assmann et.al. [2].

Observations of irradiation induced pore shrinkage and annihilation were reported in 1966 by Whapham [3] and later on by Ross [4], Bellamy and Rich [5], and Turnbull and Cornell [6, 7]. Pure fission induced densification was theoretically treated by Marlowe [8], Stehle and Assmann [9 - 12], MacEwen and Hastings [13]. Marlowe's model is based on the Coble model, where the thermally activated diffusion coefficient is substituted by an irradiation induced diffusion coefficient. The MacEwen and Hastings model assumes that pore shrinkage is caused by the annihilation of interstitials at pores. The key mechanisms in the Stehle and Assmann model are (1) the generation of an excess vacancy concentration around the pore by fission spike pore overlap, and (2) the thermally activated (except for low temperatures) migration of vacancies to the grain boundaries.

A general (thermally activated and fission induced) densification model was developed by Stehle and Assmann [21]. The relationships for densification, already published in [9 - 11] can be derived from this general model as shown below in section 4.

3. General Densification Model for Large Pores

We distinguish between large pores ($\gtrsim 0.1\,\mu m$ diameter) and small pores ($\lesssim 0.1\,\mu m$ diameter) because of a different mode of fission spike pore overlap. Large pores keep their identity and their continuous shrinkage can be described by a differential equation for the pore radius. Small pores which lie in the path of a fission fragment can spontaneously go into solution. The majority of vacancies created by this event, however, coalesce to a new pore.

For large pores, radius r, it is assumed that at the surface an equilibrium vacancy concentration is maintained which results from the equilibrium between: (1) thermally activated and fission induced vacancy generation, and (2) vacancy migration along the concentration gradient to the sink with radius R (see fig. 1). The calculation results in the following differential equation for the pore shrinkage rate [21]:

$$\frac{dr}{dt} = -\frac{(D_v^{th} + D_v^{irr})R}{r\,(R-r)} \cdot \frac{\frac{2\gamma\Omega D}{rkT}\,\frac{3\sqrt{2}}{pd} + \frac{\lambda F \omega}{3}\,(C_S - C_T)}{\frac{3\sqrt{2}}{pd}\,D_v^{th} + \frac{\lambda F \omega}{3} + \frac{(D_v^{th} + D_v^{irr})R}{r\,(R-r)}} \qquad (1)$$

D_v^{th} is the thermal vacancy diffusion coefficient in the U sublattice, D_v^{irr} is the irradiation induced vacancy diffusion coefficient, $D = D_v^{th} C_T$ is the U diffusion coefficient, γ is the surface tension, Ω is the vacancy volume, d is the spacing between the nearest neighbours in the U sublattice, λ is the length of the fission fragment path, F is the volumetric fission rate, $\omega(C_S - C_T)$ is the vacancy volume which is created by one encounter of a fission fragment with a pore, C_S is a saturation concentration, and C_T is the thermal vacancy concentration. The factor p, with $p \geq 1$, takes into account that the vacancies generated by fission fragments are injected into a certain depth of the UO_2 matrix. p jumps are necessary for recombination with the pore. The number of encounters per second for a spherical pore is given by $\frac{4\pi r^2}{3}\lambda F$ [15]. In accordance with fig. 2 we assume that a small volume of UO_2, ω, is sputtered from one side of the pore to the other during each pore penetration by a fission fragment. The same volume of UO_2 might be heavily disordered if a fission fragment passes the vicinity of the pore. In this case the stress field around the fission fragment path [14] relaxes, thus generating there an excess vacancy concentration.

Fig. 3 shows the dependence of the pore shrinkage rate on temperature, calculated according to eq. (1). The following relationships and parameters have been used:

$D_v^{th} = 0.125 \exp(-53\,000/RT)\ cm^2 s^{-1}$ [16]; $D_v^{irr} = 10^{-28} F\ cm^2 s^{-1}$ [11];

$D = 0.09 \exp(-106000/RT)\ cm^2 s^{-1}$ [10];

$R = r_g + r$, where r_g is the grain radius; $r_g = 3.10^{-4}$ cm; $r = 10^{-5}$ cm;

$p = 10^3$

$\gamma = 6.10^{-5}$ J cm^{-2}; $\lambda = 6 \cdot 10^{-4}$ cm;

$\Omega = 4.1 \cdot 10^{-23}$ cm^3; $F = 2 \cdot 10^{13}$ fiss cm^{-3}s^{-1}

$k = 1.38 \cdot 10^{-23}$ J K^{-1}; $\omega = 5 \cdot 10^{-19}$ cm^3

$d = 3.868 \cdot 10^{-8}$ cm; $C_S = 0.002$

Since vacancy generation and migration are consecutive steps pore shrinkage is determined by the slower process. Based on this, four temperature regions, depending on the fission rate, can be identified (see fig. 4):

Region I : Totally athermal densification below ≈ 450 °C

Region II : Densification depends on temperature in the region ≈ 450 °C ≦ T ≦ ≈ 750 °C, where thermally activated vacancy migration is rate controlling.

Region III: Densification is independent of temperature in the region

≈ 750 °C ≦ T ≦ ≈ 1300 °C, where athermal excess vacancy generation by fission spike pore overlap is rate controlling.

Region IV : Totally thermally activated densification above ≈ 1300 °C (so-called final stage sintering).

4. Detailed Densification Models for Large Pores

Eq. (1) can be abbreviated by:

$$\frac{dr}{dt} = - A \cdot \frac{B + C}{D + E + A} \cdot \tag{2}$$

The pore structure of UO_2 is described by homogeneously distributed pores. N_i pores per cm^3 with the initial radius r_{oi} result in an initial porosity fraction $P_{oi} = N_i \frac{4\pi}{3} r_{oi}^3$. Detailed densification models are obtained for specific relations between A, B, C, D and E by integration of the resultant simplified differential equations.

4.1 Region I and II

If at low temperatures and moderately low temperatures $E \gg A$, $E \gg D$, $C \gg B$, and if $R \gg r$, eq. (1) is simplified to the differential equation

$$\frac{dr}{dt} = - (D_v^{th} + D_v^{irr}) (C_S - C_T) \frac{1}{r} \cdot \tag{3}$$

By integration and summation over all pore classes we obtain for densification:

$$\frac{\Delta V}{V_o} = - \sum_i P_{oi} \left\{ 1 - (1 - \frac{t}{t_{oi}})^{\frac{3}{2}} \right\} , \text{ with } \frac{t}{t_{oi}} = 1 \text{ for } t \geqq t_{oi}, \tag{4}$$

$$t_{oi} = \frac{1}{(D_v^{th} + D_v^{irr}) \ (C_S - C_T)} \ r_{oi}^2 .$$

The thermally activated vacancy diffusion coefficient is $D_v^{th} = \frac{1}{6} d^2 \cdot 5 \cdot 10^4 \exp(-53\,000/RT)\ cm^2 s^{-1}$ according to Dienst [16]. The irradiation induced vacancy diffusion coefficient can be expressed by [11]:

$$D_v^{irr} = \frac{8}{3\pi^2} D_v^{(M)} \cdot \tau F \Omega_s , \tag{5}$$

where $D_v^{(M)}$ is the vacancy diffusion coefficient in the molten UO_2 ($10^{-4}\ cm^2/s$), $\tau = 2 \cdot 10^{-11}$ s is the time during which a volume of $\Omega_s = 10^{-15}\ cm^3$ around the fission fragment path is molten. With

$F = 2 \cdot 10^{13}$ fiss/cm^{3}s D_V^{irr} is in the order of magnitude of 10^{-17} cm^2/s. This value is equal to D_V^{th} at about 450 °C. C_S was determined from experimental results to be 0.002. C_T can be neclegted, because $C_S \gg C_T$.

4.2 Region III

If at moderately high temperatures $A \gg E$, $A \cong D$, $C \gg B$, and if $R \gg r$, eq. (1) is simplified to

$$\frac{dr}{dt} = -\frac{\lambda F \omega}{3} (C_S - C_T). \tag{6}$$

Integration of eq. (6) and summation yields:

$$\frac{\Delta V}{V_o} = -\sum_i P_{oi} \left\{ 1 - \left(1 - \frac{t}{t_{oi}}\right)^3 \right\}, \text{ with } \frac{t}{t_{oi}} = 1 \text{ for } t \cong t_{oi},$$
$$t_{oi} = \frac{3}{\lambda F \omega (C_S - C_T)} r_{oi}. \tag{7}$$

4.3 Region IV

If (for $R \gg r$) at high temperatures $B \gg C$, $D \gg E$, $D_V^{th} \gg D_V^{irr}$, or if $F = 0$, eq. (1) is reduced to the well known relationship

$$\frac{dr}{dt} = -\frac{2\gamma\Omega D}{kT} \frac{1}{r^2}. \tag{8}$$

By integration of eq. (8) and summation we obtain:

$$\frac{\Delta V}{V_o} = -\sum_i P_{oi} \frac{t}{t_{oi}}, \text{ with } \frac{t}{t_{oi}} \cong 1 \text{ for } t = t_{oi}, \text{ and } t_{oi} = \frac{kT}{6\Omega\gamma D(x)} r_{oi}^3. \tag{9}$$

D(x) is introduced instead of D, since the diffusion coefficient depends strongly on the stoichiometry of UO_{2+x}. Eq. (9) does not contain the grain size because of the assumption $R \gg r$ and describes the thermal densification kinetics as well as its dependence on temperature and stoichiometry completely.

5. Densification Model for Small Pores

In the model of Stehle and Assmann [12] it is assumed (see fig. 5) that inside a grain, radius r_g, a population of very fine pores (radius r_p, density Z_p) and of coarser pores (radius r_c, density Z_c) is present. Averaging the porosity, $\bar{p}$, over the grain, the following differential equation is obtained [12]:

$$\frac{d\bar{p}}{dt} = \frac{3D_v}{r_g} \left\{ \frac{C}{r}\Big|_{r = r_g} - 4\pi Z_c r_c \frac{1}{r_g^2} \int_0^{r_g} Cr^2 \, dr \right\}, \qquad (10)$$

where C is the vacancy concentration.

At moderately high temperatures (corresponding to region III), where fission induced vacancy generation is rate controlling, the solution of eq. (10) yields for the relative volume change:

$$\left(\frac{\Delta V}{V_o}\right)^f = -P_o^f \left(1 - e^{-\eta^* F \Omega_s t}\right), \qquad (11)$$

where $\eta^* = \eta^*(r_p, Z_p, r_c, Z_c, r_g)$, and Ω_s is the fission spike volume.

If only very fine pores are present within the grains, eq. (11) can be obtained by a shorter treatment reported in [9]. A pore is dispersed by a single encounter with a fission fragment. The vacancies that are formed contribute a fraction η to the densification, i.e. after the action of n fission fragments, the densification is $(1 - (1 - \eta)^n)P_o$.

6. Numerical Evaluation of In-Reactor and Thermal Densification

We give an example of the numerical evaluation for the regions III and IV because the in-reactor behaviour of LWR fuel pellets is mainly determined by region III densification; on the other hand region IV densification is used to predict in-reactor densification by thermal resinter testing. For region III and for large pores integration of eq. (6) yields (fig. 6):

$$r = r_o - 0.54 \cdot 10^{-4} \, BU \; [\mu m]. \qquad (12)$$

In region III small pores cause a relative volume decrease according to the numerical evaluated eq. (11):

$$\left(\frac{\Delta V}{V_o}\right)^f = P_o^f \left\{1 - \exp\left(-5.4 \cdot 10^{-3} \, BU\right)\right\}. \qquad (13)$$

For region IV integration of eq. (8) which is valid for all pore sizes, yields (fig. 7):

$$V_p = 4.189 \, r_o^3 - a \cdot t \; [\mu m^3]. \qquad (14)$$

In the eqs. (12) to (14) the parameters r_o, BU, P_o^f and t must be expressed in units of μm, MWd/t(U), volume fraction, and hours, respectively.

The figures in eqs. (12) to (14) have been calculated with the physical parameters already given in section 3. The thermal densification parameter "a" is dependent on temperature (see table 1) and stoichiometry. The figures reported in table 1 are valid for a O/U ratio of 2.01. According to Matzke [17] the diffusion coefficient D(x) depends on the square of x in UO_{2+x}. Therefore "a" can be adjusted by the factor $(x/0.01)^2$.

7. Experimental Results

7.1 Thermal Densification (Region IV)

An example of a confirmation of the densification kinetics corresponding to eq. 14 is shown in table 2. A fuel type with 95 % of theoretical density was heat treated in an atmosphere of 99.99 % Helium. The calculated pore size distribution fitted to the experimental results by try and error is given in table 3. The experimental results indicate that in the temperature range between 1700 and 1900 °C, for a O/U ratio of 2.01, and for maximum resinter times of about 100 h, only pores with radii smaller than 0.7 µm contribute to densification.

A more direct verification of the pore radius dependence of thermal densification is given in a result of Freshley et al. [17]. The fuel type 4 with 92.5 % TD decreased in density by 4.18 % at a resinter test for 1500 h at 1300 °C. The mean pore radius was 0.165 µm before and 0.12 µm after the resinter test.

The temperature dependence of the thermal densification was confirmed by determining the self-diffusion coefficient and comparing it with the literature (fig. 8).

7.2 In-Reactor Densification (Regions II and III)

The net volume change of UO_2 is determined by superposition of the two rate competing processes: densification and swelling. Under usual LWR conditions the matrix swelling rate is 1.1 Vol.% per 10.000 MWd/t(U). If pores with radii $r \leq 2$ µm are mainly present the curve of the net volume change as a function of burnup will go through a minimum. No minimum will be observed, if only coarse pores with radii $r \gg 2$ µm are present.

In fig. 9 the relative UO_2 column length change of an experimental unstable fuel is shown. The irradiation has been performed in the HBWR (Halden Boiling Water Reactor), Norway (IFA-418, rod 3 [19]). The continuous stack shortening versus burnup is compared with the model (Region III). The data points could be fitted by the equation inserted in fig. 9. There are only four terms: the first one represents the matrix swelling, the second one describes the disappearance of 2.55 % of submicroscopic porosity and the last two terms represent the shrinkage of two classes of coarser pores. 1.25 % and 4.00 % of pellet volume, with pore diameters of 0.5 µm and 4 µm, respectively. These findings closely agree with the real fuel structure.

Two remarks should be made in connection with this:

(1) Since the pellets have dish-shaped endfaces the length change of the fuel column is governed by the densification + swelling behaviour of an annu-

lar pellet volume. Fig. 8 indicates that in this volume region III densification was dominant. (2) Though the modeling seems to need a summation over many pore classes it is obvious that a subdivision into a few pore classes is sufficient for practical purposes.

The strong temperature dependence of densification at lower temperature levels, where vacancy migration is rate controlling (region II), has been demonstrated by an isothermal irradiation experiment in the German FR-2 (Forschungs-Reaktor-2) [20]. On a fuel type with 90 % TD it was shown that the densification rate increases by a factor of about 1.5 when the temperature is increased (from 670 °C to 710 °C) and the fission rate is decreased (from $8.3 \cdot 10^{13}$ to $4.7 \cdot 10^{13}$ fiss $cm^{-3} \cdot s^{-1}$). More extended results about temperature and fission rate dependence are reported by Freshley et.al. in [18]. Fig. 10 shows the pronounced influence of both parameters. Numerous results on fuel types as well as the evaluation of the radial distribution of porosity in irradiated fuel pellet confirm the strong dependence of the densification rate on temperature as predicted by the model.

The most important fuel property which determine densification is the pore size distribution. According to Freshley et al. [18] it can be seen in fig. 11 that initially the volume fraction of the submicron pores decreases and the volume fraction in the range between 1 and 10 µm increases. Subsequently, as irradiation continues, the volume fraction in all pore sizes below 10 µm decreases. This behaviour is predicted, in principle, by the Stehle and Assmann model [12], which assumes that part of the vacancies generated by the atomization of the small pores is captured at first by the large pores.

8. Correlations Between Thermal and In-Reactor Densification

In the IFA-418 rod 3 irradiation test described in section 7.2 the maximum relative volume decrease is about 5.25 %, whereas the thermal densification for the conditions 1600 °C/24 h and 1700 °C/24 h was 2.72 % and 3.32 %, respectively ($x = 0.01$ in UO_{2+x}). This shows that both simple tests cannot be used to predict the actual in-reactor densification exactly. Although the kinetics of thermal and in-reactor densification are different, standardized thermal resinter test can be established on the basis of the densification modeling. It can be seen from section 6.1 that one major condition for a standard resinter test is the strong control of UO_2 stoichiometry by the Oxygen partial pressure of the sinter atmosphere.

As shown in section 7.1, in [2], and in fig. 6 resintering in an inert gas atmosphere at an O/U ratio of 2.01 at temperatures between 1600 °C and 1800 °C for times between 0.5 and 100 hrs can be used to determine the amount of fine sized porosity ($r_o \approx 0.7$ µm). This fraction of the initial porosity contributes partially ($r_o \approx 0.1$ µm) to early-in-life densification according to eq. (13) or leads to a pronounced densification according to eq. (7). Pores with radii $0.7\,\mu m \approx r_o \approx 5\,\mu m$ are suitable to compensate matrix swelling. As can be seen in fig.9, 4 % of pores with a radius of 2.0 µm

shrink with a rate which is close to the matrix swelling rate of UO_2. The amount of pores with radii up to 2.0 /um can only be found by thermal densification tests at high O/U ratios. For example, all pores with r_o = 2.0 /um disappear after 17.5 hrs at 1800 °C if the O/U ratio is maintained at 2.20 by proper measures.

9. Conclusions

- In the current modeling studies the key mechanisms of densification are assumed to be the generation of excess vacancies around the pores and the annihilation of these vacancies at the grain boundaries.
- Densification shows a characteristic dependency on temperature, since both vacancy formation and vacancy migration can be predominantly thermally activated or fission induced depending on temperature (regions I to IV).
- The initial pore size distribution is the most important parameter which determines the densification rate. Large pores cause a relative volume decrease according to $\Delta V/V_o = - \sum_i P_{oi} \left\{ 1 - (1 - t/t_{oi})^n \right\}$, where n = 3/2 in regions I and II, n = 3 in region III, and n = 1 in region IV. The densification kinetics of small pores are given by $(\Delta V/V_o)^f = - P_o^f \left\{ 1 - \exp(- at) \right\}$. The interdependence of small and large pores can also be treated, in principle.
- Qualitative and partially quantitative confirmation of the general model for thermal and in-reactor densification is given in numerous experimental results. Isothermal irradiation tests are the best tool to check the predicted temperature dependence. For a direct determination of pore shrinkage kinetics quantimet analysis should be focussed on pores with radii smaller than 2 /um.
- Thermal resinter tests cannot be used to measure the actual in-reactor densification precisely, but allow the pore size distribution to be calculated which in turn determines the in-reactor densification under given conditions. Thermal densification strongly depends on the stoichiometry of UO_{2+x} and therefore the Oxygen partial pressure of the resintering atmosphere must be carefully controlled.

References

[1] COBLE, R.L., J.Appl. Phys. 32, 787 (1961)

[2] ASSMANN, H., MAIER, G., STEHLE, H., Deutsches Atomforum, Proceedings Reactor Conference, Nürnberg, p. 391 (1975)

[3] WHAPHAM, A.D., Nucl. Appl. 2, 123 (1966)

[4] ROSS, A.M., J. Nucl. Mater. 30, 134 (1969)

[5] BELLAMY, R.G., RICH, J.R., J. Nucl. Mater. 33, 64 (1969)

[6] TURNBULL, J.A., CORNELL, R.M., J. Nucl. Mater. 36, 161 (1970)

[7] TURNBULL, J.A., CORNELL, R.M., J. Nucl. Mater. 37, 355 (1970)

[8] MARLOWE, M.O., General Electric Company (USA) Report, NEDM-12175(1971)

[9] ASSMANN, H., STEHLE, H., Deutsches Atomforum, Proceedings Reactor Conference, Karlsruhe, p. 409 (1973)

[10] STEHLE, H., ASSMANN, H., J. Nucl. Mater. 52, 303 (1974)

[11] STEHLE, H., ASSMANN, H., WUNDERLICH, F., Nucl. Eng. Des. 33, 230 (1975)

[12] STEHLE, H., ASSMANN, H., J. Nucl. Mater. 61, 326 (1976)

[13] MAC EWEN, S.R., HASTINGS, I.J., Phil. Mag. 31, 135 (1975)

[14] BLANK, H., phys. stat. sol. (a) 10, 465 (1972)

[15] TURNBULL, J.A., CORNELL, R.M., J. Nucl. Mater. 41, 156 (1971)

[16] DIENST, W., Report KFK 1215 (1970), Gesellschaft für Kernforschung, Karlsruhe

[17] MATZKE, Hj., in: Plutonium and Other Actinides 1975, Eds. H.Blank, R.Lindner, North-Holland/Am. Elsevier, 1976, p. 801

[18] FRESHLEY, M.D., et.al., J. Nucl. Mater. 62, 138 (1976)

[19] GÄRTNER, M., DEWES, P., Deutsches Atomforum, Proceedings Reactor Conference, Nürnberg, p. 326 (1975)

[20] ASSMANN, H., KASPAR, G., ZIMMERMANN, H., Deutsches Atomforum, Proceedings Reactor Conference, Mannheim (1977)

[21] STEHLE, H., ASSMANN, H., to be published.

Table I Thermal densification parameter "a" for $UO_{2.01}$

Temperature °C	Parameter "a" /um^3/h
1500	$6.92 \cdot 10^{-5}$
1600	$3.27 \cdot 10^{-4}$
1700	$1.32 \cdot 10^{-3}$
1800	$4.61 \cdot 10^{-3}$
1900	$1.44 \cdot 10^{-2}$

Table II Comparison of measured and calculated thermal densification of a fuel type with an initial pore size distribution according to table III

Time hours	1700 °C		1800 °C		1900 °C	
	meas. %	calc. %	meas. %	calc. %	meas. %	calc. %
0.5	0.04	0.07	0.22	0.22	0.43	0.46
2.0	0.17	0.24	0.52	0.56	0.89	0.91
7.5	0.56	0.57	0.96	0.99	1.43	1.52
32.0	1.09	1.04	1.65	1.55	1.85	1.87
104.0	1.52	1.54	1.73	1.88	2.19	2.19

Table III Calculated initial pore size distribution of the fuel type used for the measurement reported in table II

Pore Radius r_{oi} /um	Pore Volume Fraction Poi %
0.08	0.11
0.13	0.28
0.20	0.42
0.32	0.60
0.48	0.32
0.71	0.46
≥ 1.50	2.81

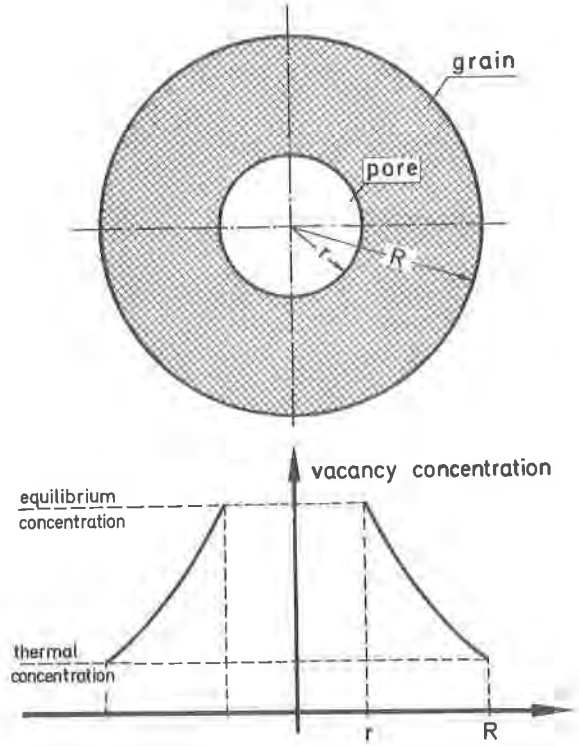

Fig. 1 Vacancy diffusion model for densification

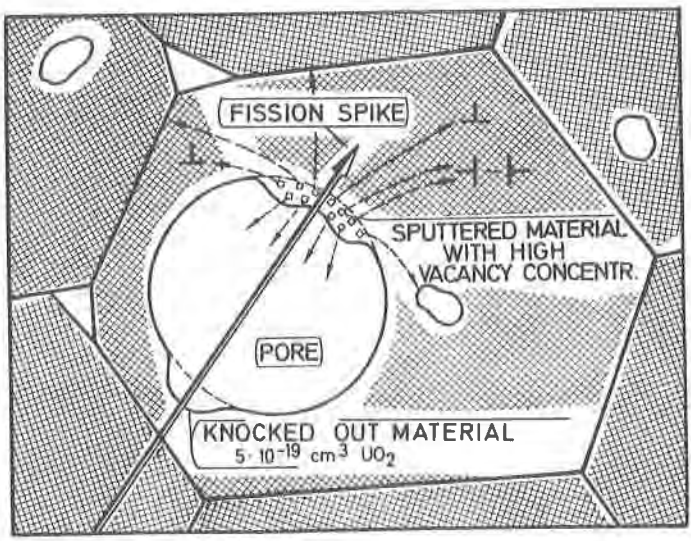

Fig. 2 Fission spike pore overlap model (large pores)

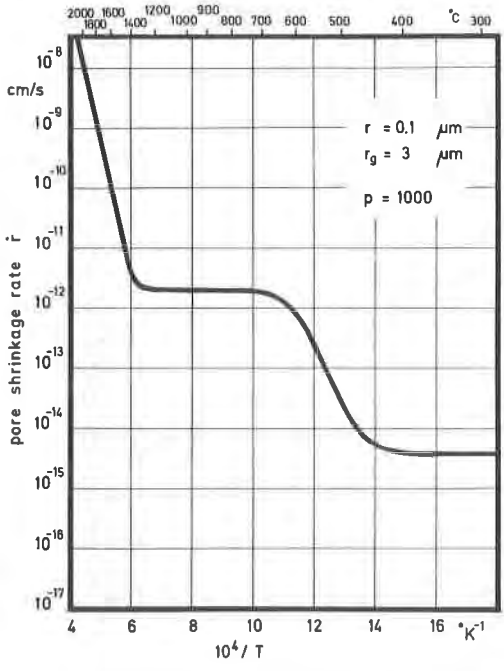

Fig. 3 Arrhenius plot for the pore shrinkage rate (large pores)

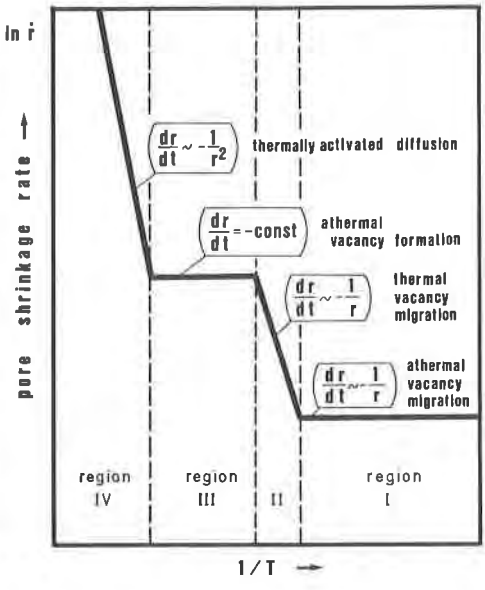

Fig. 4 Densification mechanisms in particular temperature regions (large pores)

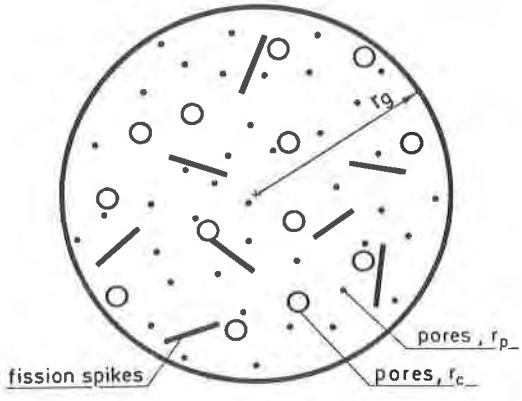

Fig. 5 In-reactor densification model (small pores)

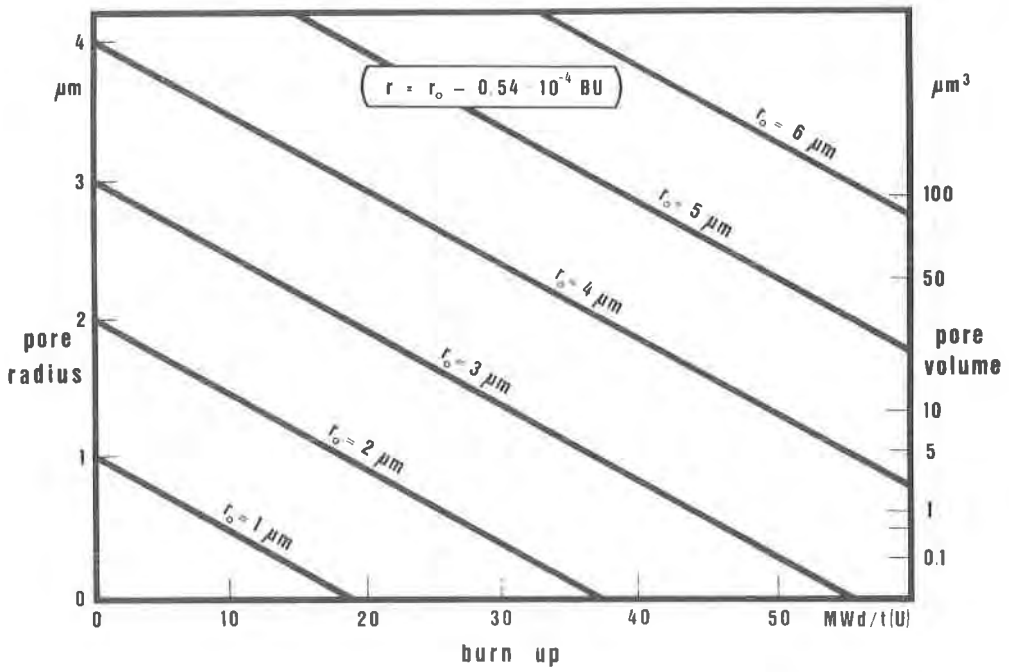

Fig. 6 In-reactor densification (large pores) in region III

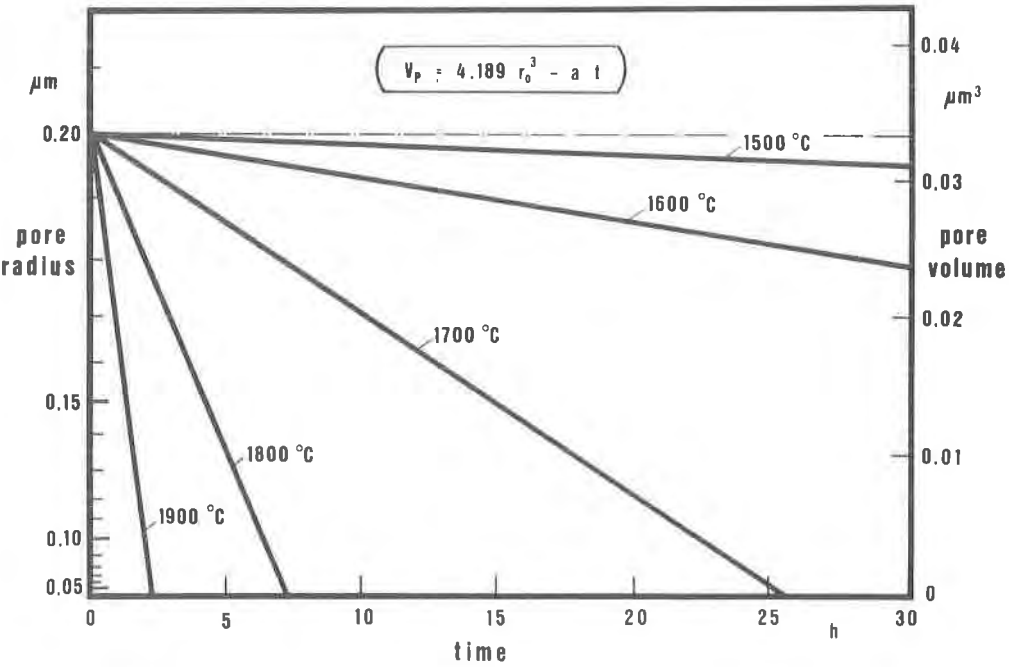

Fig. 7 Thermal densification (region IV) of UO_{2+x} (x = 0.01)

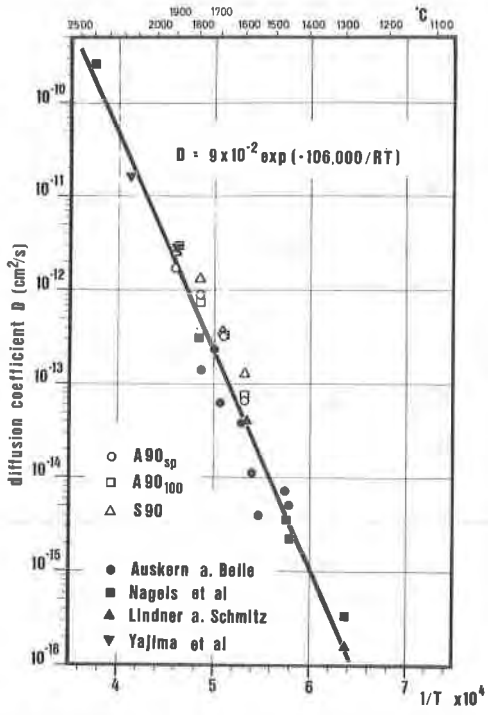

Fig. 8 Evaluation of diffusion coefficient for volume diffusion from resinter tests on UO_2 with different microstructure and comparison with the literature

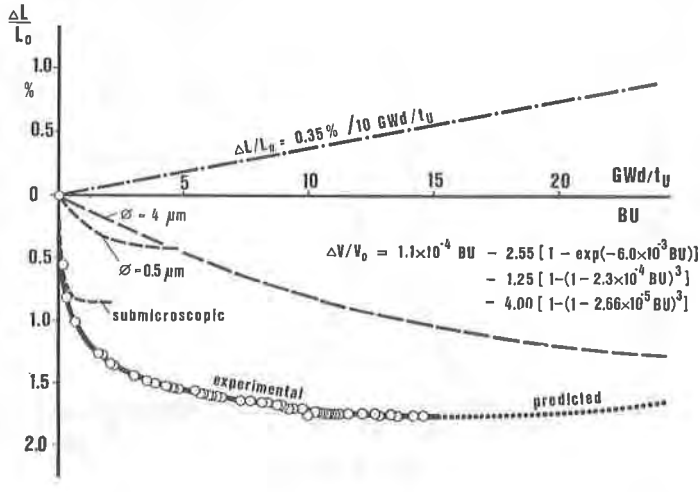

Fig. 9 Continuous stack shortening of an experimental unstable fuel (IFA 418 rod 3)
Comparison with theory

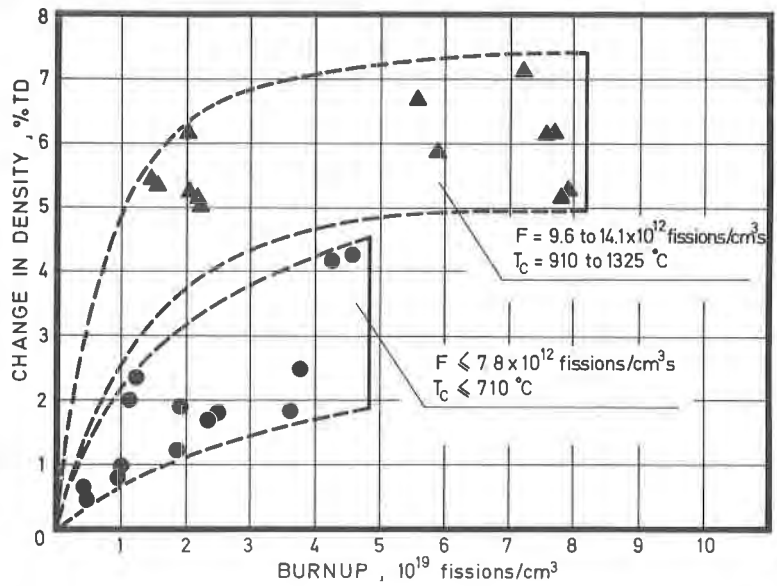

Fig. 10 Density changes of UO_2 as a function of burnup for different temperatures and fission rates (according to Freshley et al. [18])

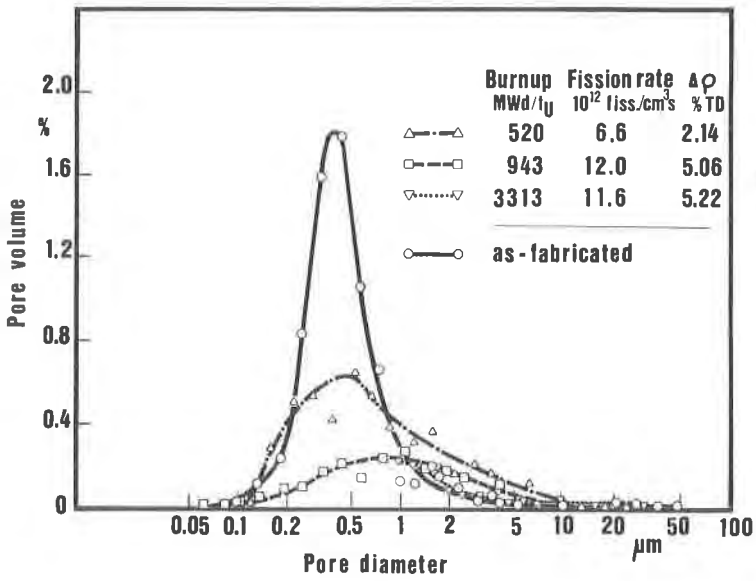

Fig. 11 Effect of irradiation on the volume distribution of porosity in an unstable UO_2 fuel type (according to Freshley et al. [18])